Ejecta detection in the middle-aged Galactic supernova remnant G296.1−0.5 observed with *Suzaku*

F. Gök,[1]⋆ A. Sezer [2,3] ⋆†

[1] *Akdeniz University, Faculty of Sciences, Department of Physics, Antalya, 07058, Turkey*
[2] *TÜBİTAK Space Technologies Research Institute, ODTU Campus, Ankara, 06531, Turkey*
[3] *Boğaziçi University, Faculty of Art and Sciences, Department of Physics, İstanbul, 34342, Turkey*

ABSTRACT

In this paper, we report the detection of ejecta in the middle-aged Galactic supernova remnant G296.1−0.5 with the X-ray Imaging Spectrometer onboard the *Suzaku* satellite. The spectra of three lobes, north, southeast and southwest and inter-lobe regions, consist of soft (0.3−2.0 keV) emission originated from non-equilibrium ionization plasma. In north, southeast and inter-lobe regions, the thermal emission can be represented by a one-component, in southwest region it can be represented by two-component non-equilibrium ionization (VNEI) model. The spectra of studied regions have lines of N, O, Ne, Mg and Si elements. Si emission from this remnant is shown for the first time in this work. Enhanced abundances of Ne, Mg and Si elements obtained show the ejecta contribution in all regions. Assuming that the remnant is in Sedov phase, we obtained ambient density $n_0 \sim 0.45$ cm^{-3}, age $t \sim 2.8 \times 10^4$ yr, shock velocity $V_s \sim 320$ km s^{-1}, shock temperature $T_s \sim 1.2 \times 10^6$ K, and swept-up mass $M_{sw} \sim 340$ M⊙ at an adopted distance of d=3 kpc.

Key words: ISM: supernova remnants−ISM: individual(G296.1−0.5)−X-rays:ISM

1 INTRODUCTION

The shell type Galactic supernova remnant (SNR) G296.1−0.5 (RA(2000) = $11^h51^m10^s$, Dec. (2000) = $-62°34'$) with 37×25 arcmin^2 angular size was discovered in radio band at 408 MHz (Clark, Caswell & Green 1973, 1975). Longmore, Clark & Murdin (1977) performed optical observation of the remnant and reported the identification of the nebulosity and its filamentary nature. Hutchings, Crampton & Cowley (1981) suggested that there was another SNR located at the northeast part of the radio remnant. Since the region in which the remnant is located on the Galactic plane is rich in SNRs, this suggestion seemed reasonable. Caswell & Bornes (1983), with an improved radio map at 408 MHz, and Bignami et al. (1986), with X-ray data from *EXOSAT* and *Einstein* observations, reported that this is a single, complex remnant. From *ROSAT* X-ray data Hwang & Market (1994) obtained an interstellar absorbtion of $N_H \geqslant 1.5 \times 10^{21}$ cm^{-2} and a low electron temperature $kT_e \sim 0.2$ keV from single temperature model fit-

ting. They also applied two temperature component model, obtained electron temperatures of ∼0.1 keV and ∼3.5 keV for each component. Assuming the distance of 4 kpc and ellipsoidal shell geometry for the remnant, they found total X-ray emitting mass and ambient density to be ∼250 M⊙ and ∼0.8 cm^{-3}, respectively. Using the Sedov equations, they found an age of ∼2×10^4 yr. From the data of *XMM-Newton* observation, Castro et al. (2011) found the electron temperature kT_e=0.6 keV by applying a non-equilibrium ionization model (VNEI) to the spectra. They obtained a low absorbing column density, $N_H = (2 - 4) \times 10^{20}$ cm^{-2}, excess of N, and a deficit of O. They suggested a massive progenitor star and concluded that the remnant was resulted from core-collapse supernova. They have detected a transient source 2XMMi J115004.8622442 at the edge of this remnant.

Various distance estimates were given from different studies; Longmore, Clark & Murdin (1977) estimated the distance d=3 ± 1 kpc by using Hα and Hβ observations and reddening measurements in the direction of crux (Miller 1972), and by fitting the radial velocity (−35 km s^{-1} with respect to the local standard of rest) to galactic rotation. From Σ−D relation Caswell & Bornes (1983), Case & Bhattacharya (1998) and Clark, Caswell & Green (1973) adopted d=7.7 kpc, d=6.6 kpc and d=4.9 kpc, respectively. Castro et al. (2011) assumed d=2 kpc, considering the giant HI

⋆ E-mail: gok@akdeniz.edu.tr   (FG);   aytap.sezer@uzay.tubitak.gov.tr (AS)
† This file has been amended to highlight the proper use of LaTeX 2$_\varepsilon$ code with the class file. These changes are for illustrative purposes and do not reflect the original paper by F. Gök.

shell, GSH 304-00-0.5 located in front of the remnant at d ~ 1.2 kpc.

Our aim is to study middle-aged SNRs to investigate interstellar medium (ISM)/shock interactions and ISM itself, i.e., the status of the ionization state, temperature (line emission) variation all over the remnant. G296.1−0.5 is particularly interesting one with its complex shock and plasma structure. The Japanese X-ray observatory *Suzaku* (Mitsuda et al. 2007), since it has a large collecting area and low background, is capable of resolving line emission characteristic of SNRs, especially at low energies, that provides valuable information in understanding SNRs. By using the archival data of *Suzaku*, we were able to produce higher quality image and the spectra of the remnant, which motivated us for this study.

This paper is organized as follows. We describe the observations and the data reduction in Section 2. In Section 3, we explain the details of image and spectral analysis. In Section 4, we discuss our results and description of the X-ray emission from G296.1−0.5.

2   OBSERVATIONS AND DATA REDUCTION

The *Suzaku* observations of the north and south regions of G296.1−0.5 were made on 2007 August 09 and on 2008 January 17, respectively, with X-ray Imaging Spectrometer (XIS: Koyama et al. (2007)). The observation ID and exposure time are 502068010, 502069010 and 77.2, 69.2 ksec, respectively. The XIS consists of four sets of X-ray CCD camera system (XIS0, 1, 2, and 3). XIS1 has a back-illuminated (BI) sensor, while XIS0, 2, and 3 have front-illuminated (FI) sensors. The XIS2 sensor was available only until 2006, therefore, we use data of XIS0, XIS1, XIS3. The XIS has a field of view (FOV) of a 17.8×17.8 arcmin^2.

In both observations, the XIS was operated in the normal full-frame clocking mode with the standard 3×3 and 5×5 editing mode. Response matrices and ancillary response files (ARFs) were generated for each XIS independently using XISSIMRMFGEN version 2007-05-14 and XISSIMARFGEN version 2008-04-05 (Ishisaki et al. 2007). Reduction and analysis of the data were performed following the standard procedure using the HEADAS v6.4 software package, and spectral fitting was performed with XSPEC v.11.3.2 (Arnaud 1996).

3   ANALYSIS

3.1   Image Analysis

Figure 1a and 1b present the smoothed XIS0 images of north and south regions of G296.1−0.5 in 0.3−10 keV energy band, respectively. In the northern part there is one bright lobe, while in the southern part there are two bright lobes. So, to determine the temperature variations and ionization states, we studied the bright lobes and a region between the lobes in the south part as shown in Fig. 1a and 1b with solid ellipses. The regions are abbreviated as north (N), southeast (SE), southwest (SW) and inter-lobe (M) region. M region is selected as the reference location in order to highlight the peculiar properties of the lobes if there is any. Dashed
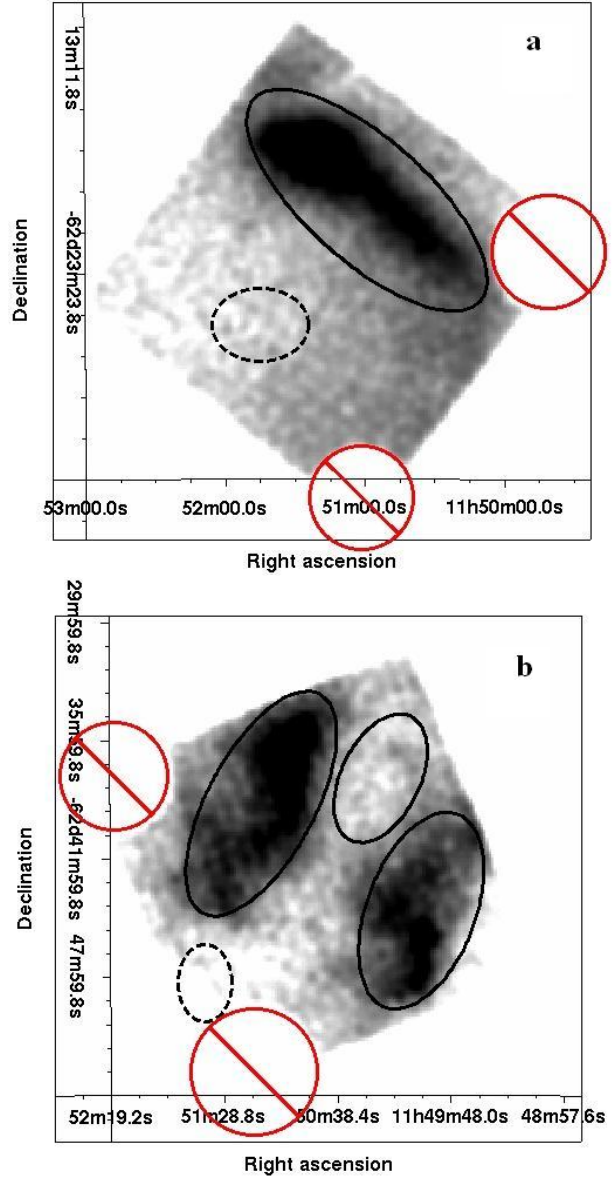

Figure 1. *Suzaku* XIS0 image of (a) N region, (b) SE, SW and M regions of G296.1−0.5 in the 0.3−10 keV energy band (gray scale). Regions for the source and the background are indicated with the solid and dashed ellipses, respectively. Two corners of each FOV, where the calibration source of ^{55}Fe is illuminated, are masked in these images. The coordinates (RA and Dec.) are referred to epoch J2000.

ellipses in both figures show the regions chosen for background subtraction. The calibration sources located at the two corners in the FOV are excluded.

Figure 2 gives the mosaic image of XIS0 in 0.3−10 keV energy band, N and S, which are overlaid with the radio image obtained at 843 MHz by Whiteoak & Green (1996) for comparison, the positions of optical filaments (Longmore, Clark & Murdin 1977), Hα emission and thin filament (Russeil & Parker 2001) and molecular material (Brand et al. 1987) are also pointed out.
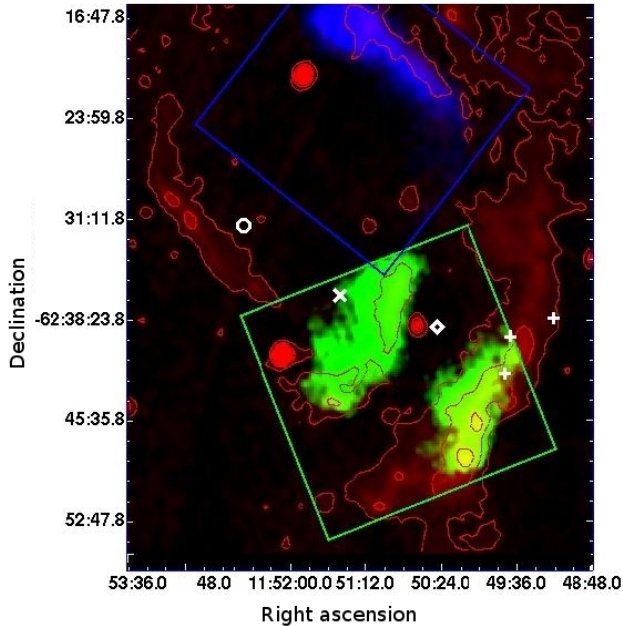
Figure 2. *Suzaku* X-ray mosaic image (blue for N and green for SE and SW) and its radio image (red) obtained at 843 MHz are overlaid and smoothed with a Gaussian kernel of σ=2 arcsec, and units are in counts s^{-1}. The linearly spaced radio contours are 0.02, 0.06, 0.10, 0.14, 0.18 and 0.22 counts/pixel. The blue and green squares indicate the XIS FOV for N and S regions, respectively. The positions of optical filaments (Longmore, Clark & Murdin 1977), Hα emission, thin filament (Russeil & Parker 2001) and molecular material (Brand et al. 1987) are marked as, plus, circle, cross and diamond, respectively. The coordinates (RA and Dec.) are referred to epoch J2000.

3.2 Spectral Analysis

We extracted the representative XIS spectra from four elliptical regions named as N, SE, SW and M (Fig. 1a and 1b) by using XSELECT version 2.4. The coordinates of the ellipses, their sizes and angles are listed in Table 1. All spectra are grouped with a minimum 20 counts bin^{-1}.

From the spectra we see that emission in 0.3−2.0 keV soft energy range is dominant and K-shell lines of N, O, Ne, Mg, and Si are present for all regions, while in 2−10 keV energy range the emission is too faint. So, we select the energy range of 0.3−2.0 keV for spectral fitting.

To analyze XIS data of the selected regions, since previous *XMM-Newton* observations showed non-equilibrium ionization (NEI) condition in this SNR, we applied NEI collisional plasma with variable abundances model (VNEI model in XSPEC, Borkowski, Lyerly & Reynolds (2001)) modified by interstellar absorption (wabs model in XSPEC, Morrison & McCammon (1983)) for all spectra. For N, SE and M regions, one-component VNEI model best describes the spectral characteristics of the emission. In the SW region, a two-component VNEI model fits (χ^2/d.o.f.=349.6/321) the emission better than a one-component VNEI model (χ^2/d.o.f.=403.6/324) statistically. During the analysis, to see if there are small scale variations the absorbing column density (N_{H}), electron temperature (kT_{e}), the ionization timescale (τ, which is often used as a key diagnostic of the NEI state, is the product of the electron density mul-

tiplied by the time after the shock heating) are allowed to vary. Since the emission lines of N, O, Ne, Mg, and Si are clearly seen in the spectra, their abundances are set as free parameters while the other elemental abundances are fixed at their solar values (Anders & Grevesse 1989). The best-fitting parameters, their errors and χ^2 values for all regions are given in Table 2 with corresponding errors at the 90 per cent confidence limit. We note that, due to better photon statistics of BI (XIS1) than FI (XIS0 and XIS3), only XIS1 results are given in this table. The background-subtracted XIS1 spectra in the 0.3−2.0 keV energy band for N, SE, SW and M regions are shown in Figure 3. We also plot the confidence contours of the absorbing column density (N_{H}) versus the electron temperature (kT_{e}) and N abundance for all regions in Figure 4. Both parameters are very well constrained for N and SE regions.

4 DISCUSSION AND CONCLUSIONS

In this paper, we give a description of the X-ray emission from G296.1−0.5 based on *Suzaku* archival data. We obtained a clear image and high quality spectra of X-ray emission that lead us detection of ejecta component in this middle-aged remnant.

The combined image, Fig. 2, shows that the remnant extends to a large area (37×25 arcmin^2) in radio band, while it is concentrated in three regions as bright lobes in X-ray band, two being in southern part and one being in the northern part. *Suzaku* observed the lobes shown by squares, not the entire remnant. Therefore we could study only the lobes and a region between SE and SW lobes. The bright X-ray emission from lobes is well correlated with radio emission. In both bands, G296.1−0.5 shows partial (irregular) shell morphology. Since radio emission is not effected by absorbtion we can say that the shape of the remnant is intrinsically anisotropic and it is interacting with a non-uniform medium. The optical imaging performed by Longmore, Clark & Murdin (1977) shows that SW region covers optical filaments with [S II]/H$\alpha \sim 1.2$ which is a typical value for shocked gas. They obtained an electron density as high as 2×10^3 cm^{-3}. Russeil & Parker (2001) detected strong localized diffuse Hα emission using the data from the Marseille survey and many thin filaments by equivalent AAO/UKST Hα survey in the direction of the remnant. Brand et al. (1987) detected molecular material with a radial velocity of ~ -38 km s^{-1} at RA(2000) = $11^{\mathrm{h}}50^{\mathrm{m}}27^{\mathrm{s}}$, Dec. (2000) = $-62°38'55''$ by using CO observations (see Fig. 2). All these observations may indicate that a shock-cloud interaction is going on and the lobes may result from these interactions.

X-ray emission of regions N, SE and M, can be described by one-component non-equilibrium ionization model (VNEI) in 0.3−2.0 keV band with electron temperature kT_{e} in the range of $(0.51 - 0.76)$ keV which is in good agreement with the recent work by Castro et al. (2011), while almost three times higher than that of Hwang & Market (1994). The ionization time scale, τ, ranges between $(1.25 - 2.46) \times 10^{10}$ cm^{-3}s indicating that the plasma in these regions is far from ionization equilibrium condition (τ is typically required to be $\geqslant 10^{12}$ cm^{-3}s for full ionization equilibrium (Masai 1984)). On the other side, in the SW region, thermal emission can be adequately described by two-component non-

equilibrium ionization model (VNEI+VNEI): the colder, $kT_e \sim 0.18$ keV, is characterized by lower solar abundances of O and N and ionization time scale $\tau \sim 5.4 \times 10^{11}$ cm^{-3}s, the hotter, $kT_e \sim 0.84$ keV, by over abundances of Ne, Mg and Si and ionization time scale $\tau \sim 1.7 \times 10^{10}$ cm^{-3}s, both components are far from ionization equilibrium condition in this region also.

The elemental abundance values of N, O, Ne, Mg and Si show small variations in N, SE and M regions. In N and SE regions, the abundance of O appears to be lower or about solar value, N, Ne, Mg and Si values are somewhat higher than solar. In general, shocked ISM spectra shows lower or about solar abundances. The plasma in these two regions contains swept-up ISM and ejecta contamination. In M region, abundance values and their errors seem somewhat higher as compared to N and SE regions (see Table 2). We note that the photon statistics in this region is poor (see Fig. 3), therefore we can say that, like N and SE regions, the plasma contains swept-up ISM and ejecta contamination. In SW region, the abundances of N and O from cold component are lower solar indicating ISM origin, while Ne, Mg and Si values from hot component are high enough to show the evidence of ejecta origin in this region also. G296.1−0.5 is a middle-aged remnant, thus the presence of ejecta at its evolved stage is not expected. However, recent X-ray observations show that in a number of middle-aged remnants metal rich ejecta are still present (e.g. G156.2+5.7 (Yamauchi et al. 1999), N49B (Park et al. 2003), IC443 (Troja et al. 2008) and Puppis A (Hwang, Petre & Flanagan 2008)). As seen in Fig. 2, the presence of molecular material in the vicinity of SE and SW regions may cause the survival of ejecta in especially these regions of this middle-aged remnant.

The absorbing column density N_H value is ranging between $(2.0 - 14.6) \times 10^{20}$ cm^{-2} across the remnant. N_H value of SW region obtained from two temperature model, $\sim 14.6 \times 10^{20}$ cm^{-2}, is in agreement with the N_H value of Hwang & Market (1994) obtained by applying two temperature model. On the other hand, N_H value of N and SE regions are $2 - 3$ times smaller than N_H value of Hwang & Market (1994) obtained by applying one temperature model, while $4 - 5$ times higher than that of Castro et al. (2011). Therefore, for our calculations we will use d=3 kpc value, that is in between the values adopted by Hwang & Market (1994) and Castro et al. (2011) and is in agreement with the value estimated by Longmore, Clark & Murdin (1977). We note that best-fitting N_H value for SW region is relatively higher than the other regions (see Table 2). The reason for this high N_H value may be the inhomogeneity of the foreground absorbing medium (see Fig. 2). Since an accurate estimate of N_H put constraints on the distance to the remnant, we obtained the confidence contours of N_H versus kT_e and N abundance as given in Fig. 4. We see that for N and SE regions both parameters are very well constrained. The X-ray flux and the corresponding luminosity values are obtained to be $F_x \sim 1.1 \times 10^{-9}$ erg s^{-1}cm^{-2} and $L_x \sim 1.2 \times 10^{36}$ erg s^{-1} at d=3 kpc in the 0.3−2.0 keV energy range.

It is suggested that most optically observed SNRs are in the adiabatic phase of their evolution (McKee & Cowie 1975). Furthermore the large physical size of this remnant, about 46 pc in radio, also suggests that it is in adiabatic expansion phase. We calculated physical parameters

of G296.1−0.5 by using information obtained by XIS images from Sedov equations (Sedov 1959):

$$R_s = 4 \times 10^{19}(\frac{t}{10^4 \text{yr}})^{2/5}(\frac{E}{10^{51}\text{erg}})^{1/5}(\frac{n_0}{1cm^{-3}})^{-1/5}\text{cm}, \quad (1)$$

$$V_s = 5 \times 10^7(\frac{t}{10^4 \text{yr}})^{-3/5}(\frac{E}{10^{51}\text{erg}})^{1/5}(\frac{n_0}{1cm^{-3}})^{-1/5}\text{cms}^{-1}, (2)$$

$$T_s = 3 \times 10^6(\frac{t}{10^4 \text{yr}})^{-6/5}(\frac{E}{10^{51}\text{erg}})^{2/5}(\frac{n_0}{1cm^{-3}})^{-2/5}\text{K}, \quad (3)$$

$$L_x = 3.3 \times 10^{29}n_0{}^2 T_e{}^{0.5} R_s{}^3 \text{ergs}^{-1}, \quad (4)$$

$$M_{\text{ISM}} = \frac{4}{3}\pi R_s^3 \mu m_H n_0, \quad (5)$$

where R_s is the shock radius, $\sim$23 pc, the explosion energy is assumed to be E_{51}=1, μ is atomic weight of 0.604, m_H is mass of a hydrogen atom. Through the equations (1−5), we obtained ambient density $n_0 \sim 0.45$ cm^{-3}, age of the remnant, $t \sim 2.8 \times 10^4$ yr, confirming that G296.1−0.5 is a middle-aged SNR. The corresponding ionization age $n_e t$ is then $\sim 2.7 \times 10^{11}$ cm^{-3}s, a plasma with this ionization age is in non-equilibrium ionization condition. Assuming the electron-ion temperature equilibration, shock velocity V_s that corresponds to best-fitting electron temperature behind the main shock front ($kT_e \sim 0.18$ keV) is calculated to be $\sim$320 km s^{-1}. Assuming uniform density for the ambient ISM, we estimated shock temperature $T_s \sim 1.2 \times 10^6$ K and the mass swept-up by the blast wave $M_{\text{sw}} \sim 340$ M$\odot$. Castro et al. (2011) suggested that G296.1−0.5 is resulted from a core-collapse supernova with a massive (> 25 M$\odot$) progenitor star. We compared our best-fitting abundances of N, O, Ne and Mg relative to Si for SE, SW and M regions with abundance ratios in core-collapse model of Woosley & Weaver (1995) and the obtained results are shown in Figure 5. As seen from the figure, we can say that the progenitor star mass might be $\gtrsim 25$ M$\odot$. Considering the high N abundance value it appears to be roughly consistent with 30 M$\odot$. When we compare this value with our estimated swept-up mass which is approximately ten times higher, we can say that G296.1−0.5 is at its critical stage and the contamination of ejecta in this middle-aged SNR is not surprising.

REFERENCES

Anders E., Grevesse N., 1989, Geochimica Cosmochimica Acta, 53, 197

Arnaud K. A., 1996, in Jacoby G., Barnes J., eds, ASP Conf. Ser. Vol.101, Astronomical Data Analysis Software and Systems V. Astron.Soc. Pac., San Francisco, p. 17

Bignami G.F., Caraveo P.A., Goldwurm A., Mereghetti S., Palumbo G.G.C., 1986, ApJ, 302, 606

Borkowski K. J., Lyerly W. J., Reynolds S. P., 2001, ApJ, 548, 820

Brand J., Blitz L., Wouterloot J. G. A., Kerr F. J., 1987, A&AS, 68, 1

Case G. L., Bhattacharya D., 1998, ApJ, 504, 761

Castro D., Slane P. O., Gaensler B. M., Hughes J. P., Patnaude D. J., 2011, ApJ, 734, 86

Caswell J.L., Bornes P.L., 1983, ApJ, 271, L55

Clark D. H., Caswell J. L., Green A. J., 1973, Nature, 246, 28

Clark D. H., Caswell J. L., Green A. J., 1975, Australian Journal of Physics, Astrophysical Supplement, 1

Hutchings J.B, Crampton D., Cowley A.P., 1981, AJ, 86, 871

Hwang U., Market T.H., 1994, ApJ, 431, 819

Hwang U., Petre R., Flanagan K.A., 2008, ApJ, 676, 378

Ishisaki Y. et al., 2007, PASJ, 59, 113

Koyama K. et al., 2007, PASJ, 59, 23

Longmore A.J., Clark D.H., Murdin P., 1977, MNRAS, 181, 541

Masai K., 1984, Ap&SS, 98, 367

McKee C. F., Cowie L. L., 1975, ApJ, 195, 715

Miller E. W., 1972, AJ, 77, 216

Mitsuda K. et al., 2007, PASJ, 59, 1

Morrison R., McCammon D., 1983, ApJ, 270, 119

Park S., Hughes J. P., Slane P. O., Burrows D. N., Warren J. S., Garmire G. P., Nousek J. A., 2003, ApJ, 592, L41

Russeil D., Parker Q.A., 2001, Publ.Astron.Soc.Aust., 18, 76

Sedov L. I., 1959, Similarity and Dimensional Methods in Mechanics, 4th edn. Academic Press, New York

Troja E., Bocchino F., Miceli M., Reale F., 2008, A&A, 485, 777

Yamauchi S., Koyama K., Tomida H., Yokogawa J., Tamura K., 1999, PASJ, 51, 13

Whiteoak J.B.Z., Green A.J., 1996, A&AS, 118, 329

Woosley S. E., Weaver T. A., 1995, ApJS, 101, 181

Table 1. Centre coordinates, sizes and angles of N, SE, SW, M and background regions.

Regions	Centre Coordinates RA(2000) ; Dec. (2000) (h m s ; ° ′ ″)	Size (arcmin)	Angle (degrees)
N	11 50 59 ; −62 19 46	7.5 × 3.0	318
Background[a]	11 51 45 ; −62 25 56	2.4 × 1.8	0
SE	11 51 12 ; −62 39 13	2.7 × 6.3	332
SW	11 50 02 ; −62 44 38	2.8 × 5.2	339
M	11 50 20 ; −62 37 55	1.9 × 3.5	334
Background[b]	11 51 37 ; −62 48 19	1.4 × 1.9	0

[a] for N region;
[b] for S region.

Table 2. Best spectral fitting parameters of XIS1 spectra obtained for N, SE, SW and M region of G296.1−0.5 in 0.3−2.0 keV with corresponding errors at 90 per cent confidence level.

Component	Parameters	N	SE	SW	M
Absorbtion	$N_{\mathrm{H}}(\times 10^{20}\ \mathrm{cm}^{-2})$	7.5 ±0.5	4.7 ±0.6	14.6 ±1.4	2.0 ±0.5
VNEI	kT_{e}(keV)	0.58 ±0.02	0.51±0.02	0.18±0.01	0.76±0.15
Abundance[a]	N	1.91 ±0.07	2.15 ±0.09	0.75 ±0.12	3.08 ±0.36
	O	0.81 ±0.02	1.01 ±0.03	0.39 ±0.03	0.91 ±0.07
	Ne	1.56 ±0.04	1.92 ±0.05	(1)	2.3±0.2
	Mg	1.37±0.06	1.44±0.10	(1)	2.3±0.5
	Si	1.26±0.21	1.75±0.36	(1)	2.7±1.4
	$n_{\mathrm{e}}t(\times 10^{10}\ \mathrm{cm}^{-3}\mathrm{s})$	2.24 ±0.15	2.46±0.21	54.2±1.3	1.25±0.29
	E.M.[b]	5.8±1.2	4.6±1.1	89.3±10.2	0.59±0.03
VNEI	kT_{e}(keV)	-	-	0.84±0.09	-
	Ne	-	-	2.38±0.31	-
	Mg	-	-	1.55±0.21	-
	Si	-	-	2.39±0.55	-
	$n_{\mathrm{e}}t(\times 10^{10}\ \mathrm{cm}^{-3}\mathrm{s})$	-	-	1.68±0.14	-
	E.M.	-	-	1.8±0.4	-
	χ^2/d.o.f.	619.2/380=1.63	590.2/338=1.75	349.6/321=1.09	202.7/185=1.09

[a] Abundance ratio relative to the solar value (Anders & Grevesse 1989), (1) indicates that the elemental abundance is fixed at solar.
[b] Emission measure EM=$\int n_{\mathrm{e}} n_{\mathrm{H}} \mathrm{d}V$ in the unit of 10^{57} cm^{-3}, where n_{e} and n_{H} are number densities of electrons and protons, respectively and V is the X-ray-emitting volume.
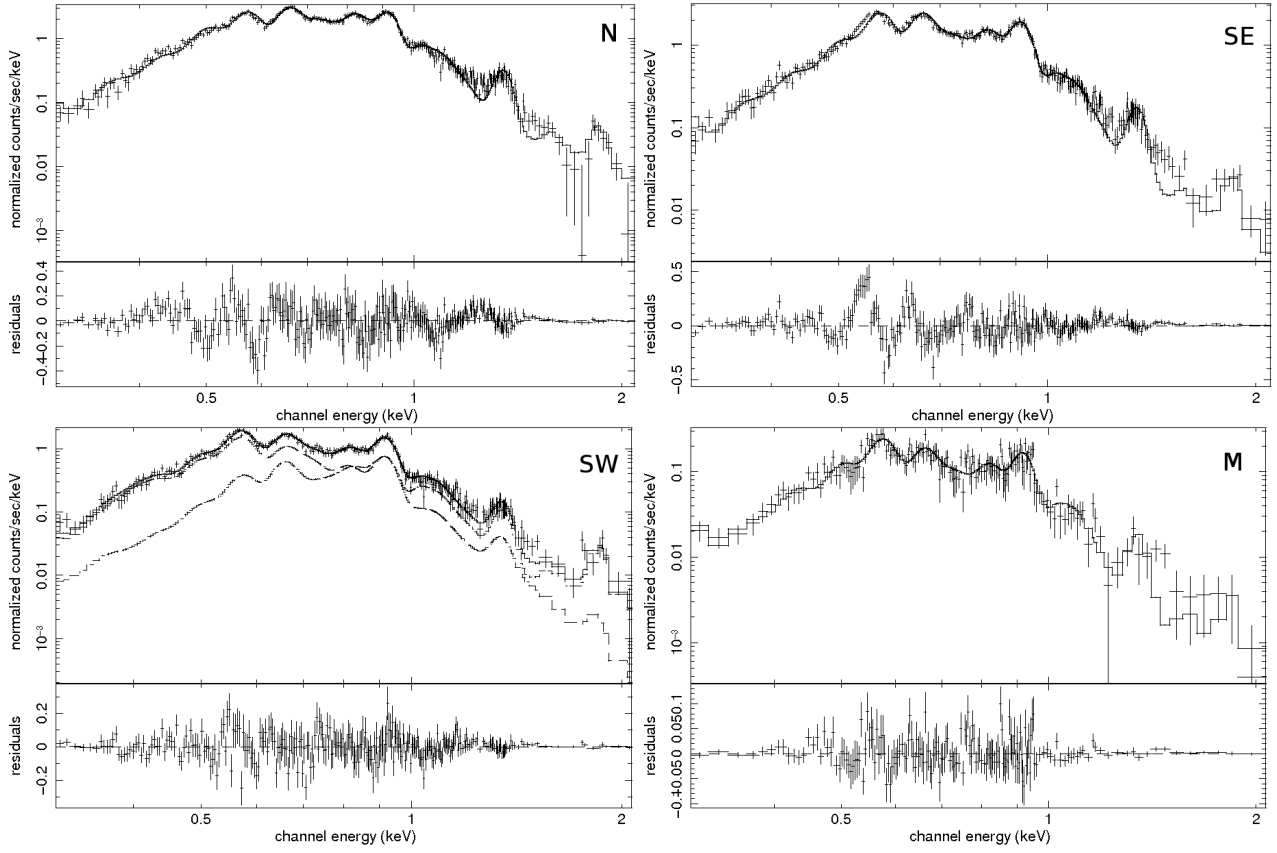
Figure 3. XIS1 spectra of G296.1−0.5 obtained in the 0.3−2.0 keV energy band. The indicated fits consists of an absorbed VNEI model for N, SE and M regions and an absorbed VNEI+VNEI model for SW region. The bottom window gives the residuals from the best-fitting model for XIS1 spectra.
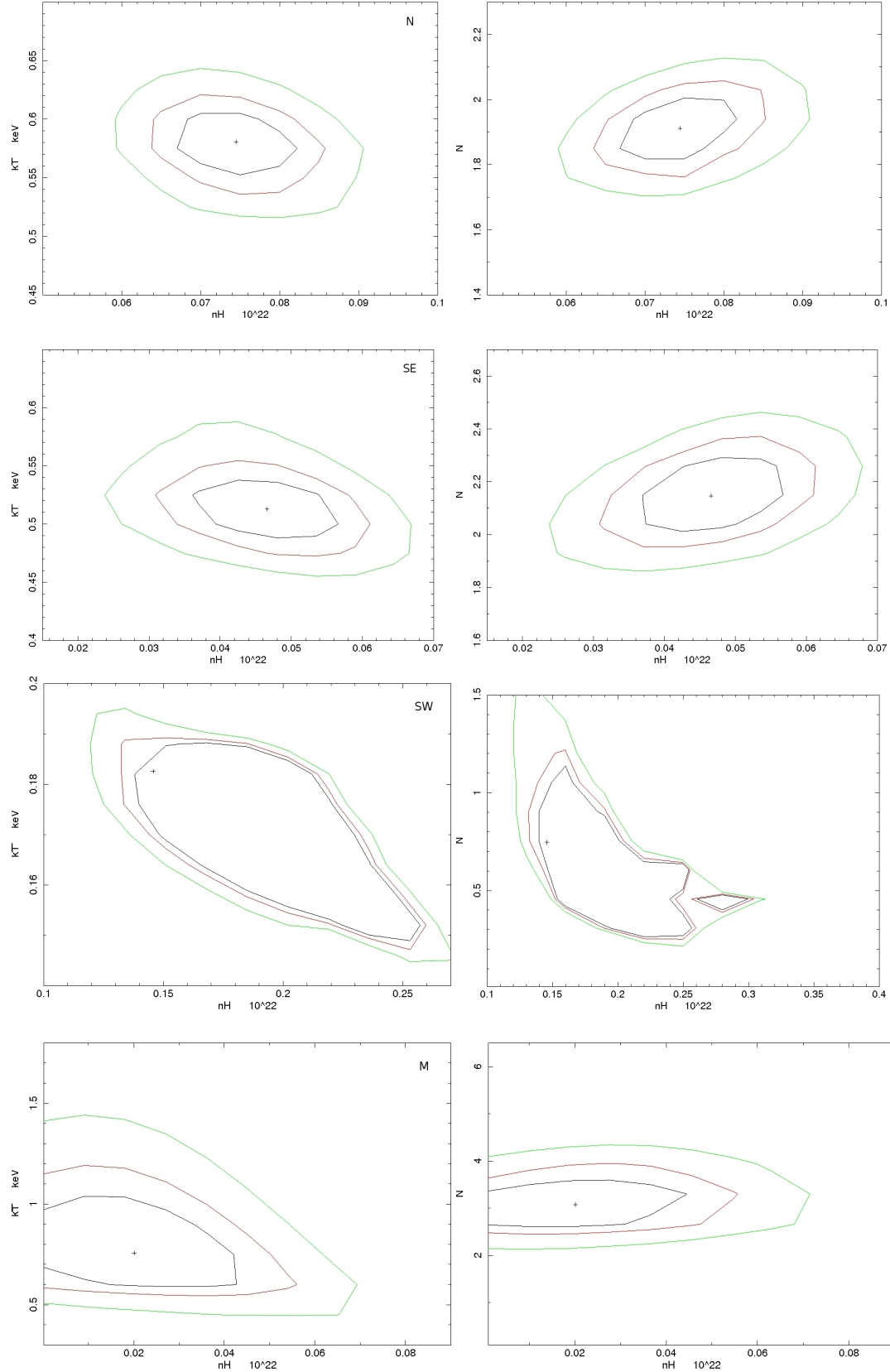
Figure 4. Confidence contours of N_{H} versus kT_{e} (left) and N_{H} versus N abundance (right) spectral fitting for all regions of G296.1−0.5. The contours are at the 68, 90 and 99 per cent confidence levels. The parameter values corresponding to the best-fitting are marked by a plus sign (+).
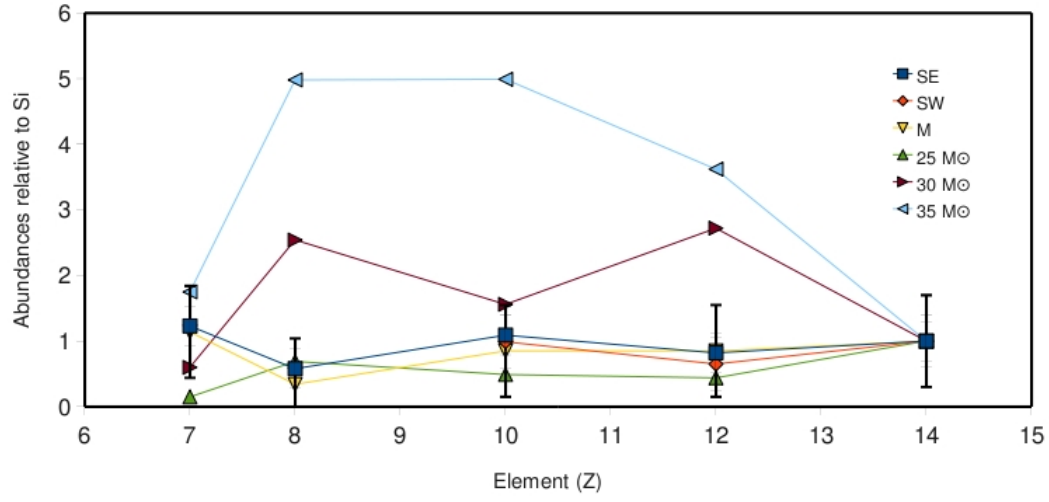
Figure 5. Best-fitting abundances of N, O, Ne and Mg relative to Si relative to solar (for SE, SW and M regions) are compared with the theoretical predictions of core-collapse model (Woosley & Weaver 1995) with 25, 30 and 35 M⊙ progenitors.